JOURNAL OF THE MECHANICAL BEHAVIOR OF BIOMEDICAL MATERIALS 29 (2014) 339–349

Available online at www.sciencedirect.com

ScienceDirect

www.elsevier.com/locate/jmbbm

Research Paper

Effect of storage on tensile material properties of bovine liver

*Yuan-Chiao Lu, Andrew R. Kemper, Costin D. Untaroiu**

Virginia Tech and Wake Forest University School of Biomedical Engineering and Sciences, Blacksburg, VA 24060, USA

ARTICLE INFO

Article history:
Received 30 May 2013
Received in revised form
18 September 2013
Accepted 22 September 2013
Available online 8 October 2013

Keywords:
Liver
Parenchyma
Failure
Tensile test
Material model
Freezing Tissue preservation

ABSTRACT

Cadaveric tissue models play an important role in the assessment and optimization of novel restraint systems for reducing abdominal injuries. However, the effect of tissue preservation by means of freezing on the material properties of abdominal tissues remains unknown. The goal of this study was to investigate the influence of frozen storage time on the material responses of the liver parenchyma in tensile loading.

Specimens from ten bovine livers were equally divided into three groups: fresh, 30-day frozen storage, and 60-day frozen storage. All preserved specimens were stored at −12 °C. Dog-bone specimens from each preservation group were randomly assigned to one of three strain rates (0.01 s^{-1}, 0.1 s^{-1}, and 1.0 s^{-1}) and tested to failure in tensile loading. The local material response recorded at the tear location and the global material response of the whole specimen of the liver parenchyma specimens were investigated based on the experimental data and optimized analytical material models.

The local and global failure strains decreased significantly between fresh specimens and specimens preserved for 30 days ($p<0.05$), and between fresh specimens and specimens preserved for 60 days ($p<0.05$) for all three loading rates. Changes on the material model parameters were also observed between fresh and preserved specimens. Preservation by means of frozen storage was found to affect both the material and failure response of bovine liver parenchyma in tensile loading. The stiffness of the tissue increased with increased preservation time and increased strain rate.

In summary, significant changes ($p<0.05$) between the failure strain of previously frozen liver parenchyma samples and fresh samples were demonstrated at both global and local levels in this study. In addition, nonlinear and viscoelastic characteristics of the liver parenchyma were observed in tension for both fresh and preserved samples.

1. Introduction

The liver is the largest abdominal organ in the human body and while it is within a relatively protected location, it is one of the most commonly injured intra-abdominal organs as a result of blunt trauma (Brammer et al., 2002). Abdominal injuries caused by motor vehicle collisions have severe consequences (Arajarvi et al., 1987; Cheynel et al., 2011; Greingor and Lazarus, 2006), and the liver is one of the most frequently injured abdominal organs in frontal vehicle crashes (Elhagediab Rouhana, 1998). In addition, mortality and morbidity rates increase with the severity grade of liver

*Corresponding author. Tel.: +1 540 231 8997; fax: +1 540 231 2953.
E-mail addresses: costin@vt.edu, costin.untaroiu@gmail.com (C.D. Untaroiu).

1751-6161/$ - see front matter © 2013 Elsevier Ltd. All rights reserved.
http://dx.doi.org/10.1016/j.jmbbm.2013.09.022

injuries (Brammer et al., 2002). While the material properties of liver tissue has been investigated, most of the previous studies tested only fresh human or animal liver tissue (Brunon et al., 2010; Bummo and Jung, 2007; Chui et al., 2007; Kemper et al., 2010). However, the majority of biomechanical tests used to characterize the response and injury tolerance of the human abdomen are performed on fresh, previously frozen post-mortem human surrogates (PMHS) (Crandall et al., 2011; Eichberger et al., 2000; McIntosh et al., 2007; Salzar et al., 2009; Untaroiu et al., 2012). Consequently, there is a need to better understand the potential changes in the material properties of the liver tissue due to preservation by means of freezing.

In the recent years, PMHS have served as invaluable tools for the characterization of human biomechanical responses during impact loading (Crandall, 1994; Crandall et al., 2011). Therefore, the development of reliable preservation methods for PMHS, which minimize the biomechanical differences between living humans and preserved PMHS, has become very important for biomechanics research. During the late 1960s, it was shown that the embalming process changes the response of human tissues (Crandall, 1994). As a result of these findings, the testing of embalmed PMHS was abandoned. From this point, freezing and refrigeration methods have been widely used to store and preserve unembalmed post-mortem tissue. Typically, freezer storage methods are used to preserve post-mortem tissue at temperatures ranging from −10 °C to −70 °C. Various studies have shown that freezing within this range does not have a effect on the biomechanical response of bone or collagenous tissues such as ligaments or intervertebral discs (Frankel, 1960; Griffon et al., 1995; Hamer et al., 1996; Linde and Sorensen, 1993; Sedlin, 1965; Smeathers and Joanes, 1988; Weaver, 1966; Woo et al., 1986). While several studies have reported some comparisons between the mechanical properties of fresh and previously frozen abdominal organ tissues (Hollenstein et al., 2006; Ocal et al., 2010; Tamura et al., 2002), the effect of freezing on the mechanical response of the liver tissue under different loading rates is still largely unknown.

A number of studies have investigated the effects of freezing on the responses of animal livers under different types of loading schemes. Brunon et al. (2010) conducted quasi-static tensile failure tests on both fresh and previously frozen porcine liver parenchyma and capsule samples, and found that freezing affects the failure properties of porcine liver capsule but not human liver capsule. Ocal et al. (2010) conducted compressive impact experiments on bovine liver specimens to investigate the effect of preservation period (1–48 h after harvesting) on the viscoelastic material properties and found that liver tissue becomes stiffer and more viscous as the preservation time increases. Santago et al. (2009) compared the tensile failure stress and failure strain of fresh bovine liver parenchyma and bovine liver parenchyma frozen for 26 days and concluded that freezing decreased the failure strain. However, the study by Santago et al. (2009) was limited to samples obtained from only one bovine liver and the evaluation of a single loading rate. Nguyen et al. (2012) investigated the influence of a freeze-thaw cycle on the stress–stretch curves of porcine liver and reported that the mechanical properties of the liver tissues were almost unaffected by the freeze-thaw cycle. Tamura et al. (2002) performed a series of pre-conditioning compression tests on fresh and previously frozen porcine liver specimens and determined that freezing had no effects on the mechanical response of the tissue. However, it is possible that damage to the tissue during the pre-conditioning may have masked any potential changes in the compressive response resulting from the freezing process. Lu and Untaroiu (2013) conducted indentation tests on fresh porcine liver and porcine liver frozen for 20 days and found that freezing did not change the stiffness of porcine liver.

Although there have been some studies that have investigated the effect of freezing on liver tissue, the conclusions regarding the effect of freezing on the material response of liver tissue varies between studies. The discrepancies between these studies could potentially be due to variability in the composition of the liver tissues between mammalian species, the preservation periods evaluated, the loading rates, or the mechanism of loading. Previous studies have shown that the tensile material properties of bovine liver are not significantly different from those of human liver (Kemper et al., 2010). Therefore, the purpose of the current study was to investigate the influence of freezing on the biomechanical responses of the bovine liver parenchyma in tensile loading.

2. Method

2.1. Sample source and preservation

Uniaxial tensile tests were performed on the parenchyma of 10 fresh bovine livers obtained from Animal Technologies (Tyler, Texas, USA) (Fig. 1). Each organ was sectioned into three equal portions: one was tested immediately upon receipt; one tested after 30 days of frozen storage (Day 30); and one tested after 60 days of frozen storage (Day 60). The bovine livers were received within 24 h after slaughter. During transportation, the livers were sealed in plastic bags, and stored in ice filled containers. Frozen specimens were stored in a sealed container at −12 °C (Lu and Untaroiu, 2013), and then tested under the same testing condition as fresh samples after thawing. The time between the start of the thawing process and the testing was approximately 12 h. Frozen-thawed specimens were evaluated in this study because previously frozen PMHS are commonly used in abdominal impact tests (Untaroiu et al., 2012). The 30–60 day time interval reasonably approximates to the time window required to obtain serology, required approval, and pre-test medical examinations for PMHS.

2.2. Sample preparation and experimental setup

The tissue slicing and stamping procedures described by Kemper et al. (2010, 2012) were used to obtain constant thickness “dog-bone” shaped liver parenchyma specimens (thickness: ~5 mm, gage length: 19 mm, gage width: 10 mm) commonly used for uniaxial tensile testing . The specimens were prepared such that longitudinal axis of each specimen was parallel to the liver surface during the stamping process. All samples were then immersed in a bath of Dulbecco's

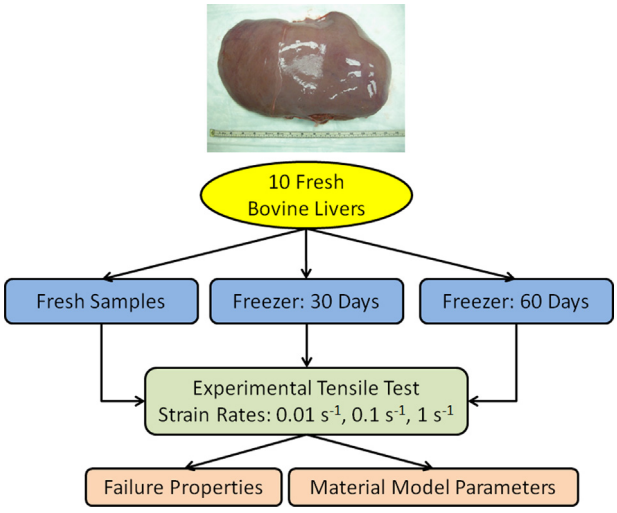

Fig. 1 – Overall testing procedure.

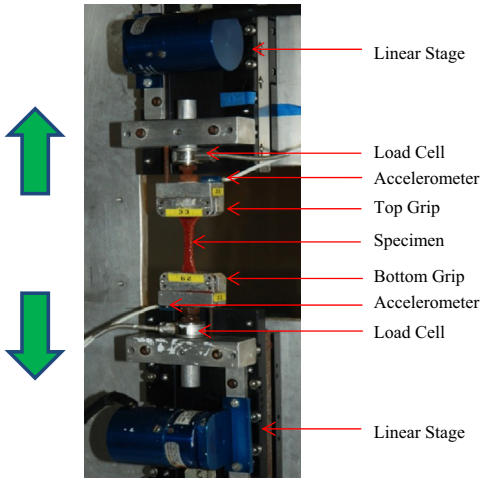

Fig. 2 – Experimental setup.

Modified Eagle's Medium to maintain specimen hydration until testing. Specimens from each group (fresh, Day 30, and Day 60) were divided into three sets which were tested until failure at one of strain rates: (0.01 s^{-1}, 0.1 s^{-1}, or 1.0 s^{-1}) in order to characterize the strain-rate dependent characteristics of the tissue over a large range of strain rates (Fig. 1). It should be noted that these strain rates are consistent with rates used in similar publications (Kemper et al., 2010, 2012).

The tensile testing system consisted of two motor driven linear stages (Parker Daedal MX80S, Irwin, PA) mounted to a vertically oriented aluminum plate (Fig. 2). A uniaxial load cell (Interface, WMC Miniature-22.24N, Scottsdale, AZ) and an accelerometer (Endevco 7264B, 2000G, San Juan Capistrano, CA) were mounted between the linear actuator and the clamp. The system was operated with a multi-axis controller (Parker ACR9000, Irwin, PA), which provided synchronized motion of both linear stages, and a motor driver (Parker ViX, Irwin, PA). The specimen mounting procedure described by Kemper et al. (2010, 2012) was used to ensure that all specimens had a minimal but consistent preload (i.e. 1 g of tension caused by gravity). The testing system loaded the specimen by simultaneously moving the top and bottom grips away from one another at a constant velocity. A typical uniaxial test failure is shown in Fig. 3. The force and displacement time histories were recorded during each test, along with high-speed video. The data acquisition and video sampling rates for each loading rate are listed in Table 1. The testing temperature was chosen to be normal room temperature (24 °C), which is representative of the temperature used during PMHS abdominal impact tests.

2.3. *Data analysis*

The material response of the specimens was analyzed using local and global models (Fig. 4). The local model (LM) approximated the specimen as a beam with the length corresponding to the closest optical markers spanning the location of the tear and constant initial cross-sectional area at the tear region located in the middle region of the specimen (i.e. the gage length). The initial cross-sectional area at the region of the tear was quantified by first determining the location of the failure in the high-speed video and then determining the initial width and thickness at that location from the pre-test pictures. The optical markers were tracked throughout the duration of the test using motion analysis software (TEMA Version 2.6, Linkoping, Sweden). The displacement between these markers was curve fit with a 5th degree polynomial up to the time of failure (average R^2= 0.936) to reduce the measurement noise. This methodology is consistent with that used by previous studies (Kemper et al., 2010, 2012). The global model (GM) approximated the specimen as a beam with the specimen length corresponding to distance between the clamps and constant initial cross-sectional area. The global displacement between the grips was measured during tests using potentiometers attached to the linear stages and then fit with a 1st degree polynomial (average R^2=0.999) to reduce the measurement noise. The initial cross-sectional area was calculated from pre-test pictures as the average of the cross-sectional areas at three locations: the middle location, 3 mm above the middle location, and 3 mm below the middle location.

The stretch ratio (λ) and Green-Lagrangian (GL) strain (ε) of LM and GM were then calculated from the curve fit displacement data as follows:

$$\lambda = \frac{L_n}{L_0} \tag{1}$$

$$\varepsilon = \frac{1}{2}(\lambda^2 - 1) \tag{2}$$

where L_0 is the initial distance between the optical markers (LM) or the initial distance between clamps (GM). L_n is the instantaneous distance between the optical markers (LM) or instantaneous distance between the clamps (GM). The strain rates for LM and GM were calculated as the slope, from 25% to 75% of the failure strain, of the time histories of the local strain and global strain correspondingly (Kemper et al., 2010, 2012).

The inertial force added by the grip/load cell was calculated based on grip acceleration (a), and effective mass (m_{eff}). The effective mass was defined as half of the load cell mass plus the grip mass between the load cell and specimen. For

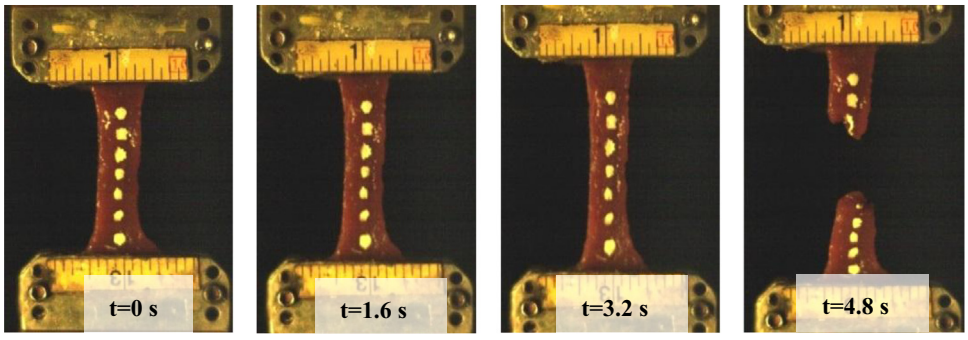

Fig. 3 – High-speed video stills of a typical uniaxial tensile test (Fresh, Rate 2: 0.1 s^{-1}).

Table 1 – Data acquisition and video sampling rates by loading rate.

Rate	Desired strain rate (s^{-1})	Data acquisition (kHz)	Video (Hz)
Rate 1	0.01	0.2	20
Rate 2	0.1	2.0	70
Rate 3	1.0	20.0	500

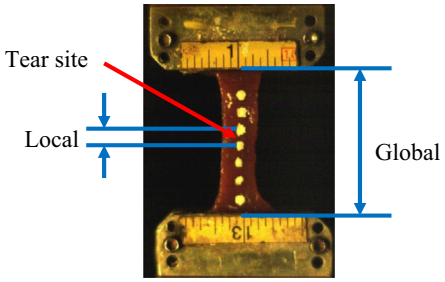

Fig. 4 – An illustration of the local and global sites for the stretch ratio calculation.

the two lowest strain rates (0.01 s^{-1} and 0.1 s^{-1}), the inertial force was negligible, so the measured force was not inertially compensated. For the highest strain rate (1.0 s^{-1}), the measured force was inertially compensated (Eq. 3) because of the higher levels of the inertial force (under the level of 5% of the measured force – F) were observed. Finally, the force (F for 0.01 s^{-1} and 0.1 s^{-1}; F_{IC} for 1.0 s^{-1}) was fit with a 5th degree polynomial function up to the time of failure (average R^2=0.890).

$$F_{IC} = F - am_{eff} \tag{3}$$

The 2nd Piola–Kirchhoff (PK) Stress (S) is a symmetric tensor usually employed for characterization of materials with large deformation, and is the energy conjugate of the GL strain tensor. In the case of uniaxial test, the 2nd PK Stress (S) was calculated based on the curve fit force data, the stretch ratio (λ), and initial cross-sectional area (A_0) (Eq. (4)).

$$S = \frac{F}{\lambda A_0} \text{ for } 0.01\ s^{-1} \text{ and } 0.1\ s^{-1};\ \text{for } 1.0\ s^{-1} \tag{4}$$

The failure stress and failure strain were defined as the stress and strain at the time of failure. The time of failure was defined as the point of peak load preceeding a significant decrease (>3%) in the load. This corresponded to the timing of the initiation of the failure tear when the initiation of the failure tear could not be observed in the video (Kemper et al., 2010, 2012). The stress–strain curves were then calculated for each test. The average curves were calculated for each combination of strain rates and fresh/preservation methods using a normalization technique (Lessley et al., 2004). An elliptical corridor approach was used to account for variability in both stress and strain coordinates along the average curves (Untaroiu and Lu, 2013). The boundaries of the elliptical corridor were obtained as an envelope of the ellipsoids defined along the average curves using 1 standard deviation (±1 S.D.) as ellipsoid axes.

2.4. *Material modeling of liver parenchyma*

An optimization procedure was employed to identify the material model properties of both fresh and preserved tissues, which may be implemented later in human finite element (FE) models and used to simulate impact events. Abdominal tissues, such as liver, are commonly assumed to be isotropic and incompressible materials (Hu et al., 2009; Nava et al., 2008; Nguyen et al., 2012). A hyperelastic model called the Ogden material model (Ogden, 1997), which is frequently used to model soft tissue (Hu et al., 2009, 2011; Klinich et al., 2012), was utilized for material characterization of liver parenchyma as it demonstrated the closest match to the test data compared to other hyperelastic material models implemented in LS-Dyna v. 971 (Untaroiu and Lu, 2013). The strain energy function of the Ogden incompressible material model (Ogden, 1997) is expressed as

$$W(\lambda_1,\lambda_2,\lambda_3) = \sum_{i=1}^{M} \frac{\mu_i}{\alpha_i}(\lambda_1^{\alpha_i} + \lambda_2^{\alpha_i} + \lambda_3^{\alpha_i} - 3) \tag{5}$$

where λ_1, λ_2,λ_3 are the principal stretches, M is the order of the Ogden material model, μ_i and α_i are the ith shear modulus and exponent, respectively. For an isotropic incompressible material with an applied stretch λ_1 along the loading direction, the stretches along the other two orthogonal directions are

$$\lambda_2 = \lambda_3 = \lambda_1^{-1/2} \tag{6}$$

The strain energy function of a first-order Ogden model (M=1) can therefore be expressed as

$$W(\lambda_1) = \frac{\mu_1}{\alpha_1}(\lambda_1^{\alpha_1} + 2\lambda_1^{-\alpha_1/2} - 3) \tag{7}$$

The 2nd PK stress of the Ogden model (S_1) is then given by

(Holzapfel, 2000)

$$S_1 = \frac{\partial W}{\lambda_1 \partial \lambda_1} \tag{8}$$

Therefore, the time history of the force predicted by the model in the specimen is

$$F_m(t) = \lambda_1 S_1(\mu_1, \alpha_1, t) A_0 \tag{9}$$

The values of the material model parameters (α_1 and μ_1) were optimized using the active-set algorithm in MATLAB v. R2012b (The MathWorks, Inc., Natick, MA), which tried to minimize the root mean square (RMS) of the differences between the model force to the corresponding test data (Eq. (10)).

$$F_{error} = \sqrt{\sum_{i=1}^{n} [F_m(t_i) - F_{IC}(t_i)]^2} \tag{10}$$

where t_i is a series of n-time sequences equally distributed from the time when the specimen started to be loaded (time 0) up to the time of failure. The active-set algorithm utilizes a sequential quadratic programming method typically used to solve medium scale optimization problems (problems with reduced number of variables) (Coleman, 2011). The initial values of α_1 and μ_1 were chosen as 10 and 5 kPa, respectively (Untaroiu and Lu, 2013). The parameters (α_1 and μ_1) were optimized for each average stress–strain curve of each combination of the three loading rates and three preservation times (fresh, Day 30, and Day 60). The ground-state shear modulus μ can then be determined by (Hu et al., 2011)

$$\mu = \frac{\mu_1 \alpha_1}{2} \tag{11}$$

2.5. Statistical analysis

A series of two-sample Mann–Whitney tests for the difference in median were performed to evaluate significance (α=0.05) in failure stress, failure strain, and optimized material properties between storage times and between loading rates. When comparing the failure properties between local and global stretch ratio data sets, paired two sample t-tests were utilized (α=0.05).

3. Results

The characteristic averages and elliptical corridors for the stress-strain curves of fresh, Day 30, and Day 60 specimens are shown in Fig. 5 by loading rate. The average strain rates were 0.007 s^{-1}, 0.071 s^{-1}, and 0.684 s^{-1} for LM and 0.009 s^{-1}, 0.091 s^{-1}, and 0.914 s^{-1} for GM for specimens tested Rate 1 (0.01 s^{-1}), Rate 2 (0.1 s^{-1}), and Rate 3 (1.0 s^{-1}), correspondingly. The data show that the tissue stiffness and failure stress of both LM and GM increased as a result of freezing for all loading rates, while failure strain of both LM and GM decreased. The number of samples in each group is shown in Fig. 6a.

The averages and standard deviations of failure strain and failure stress for both LM and GM are shown by loading rate

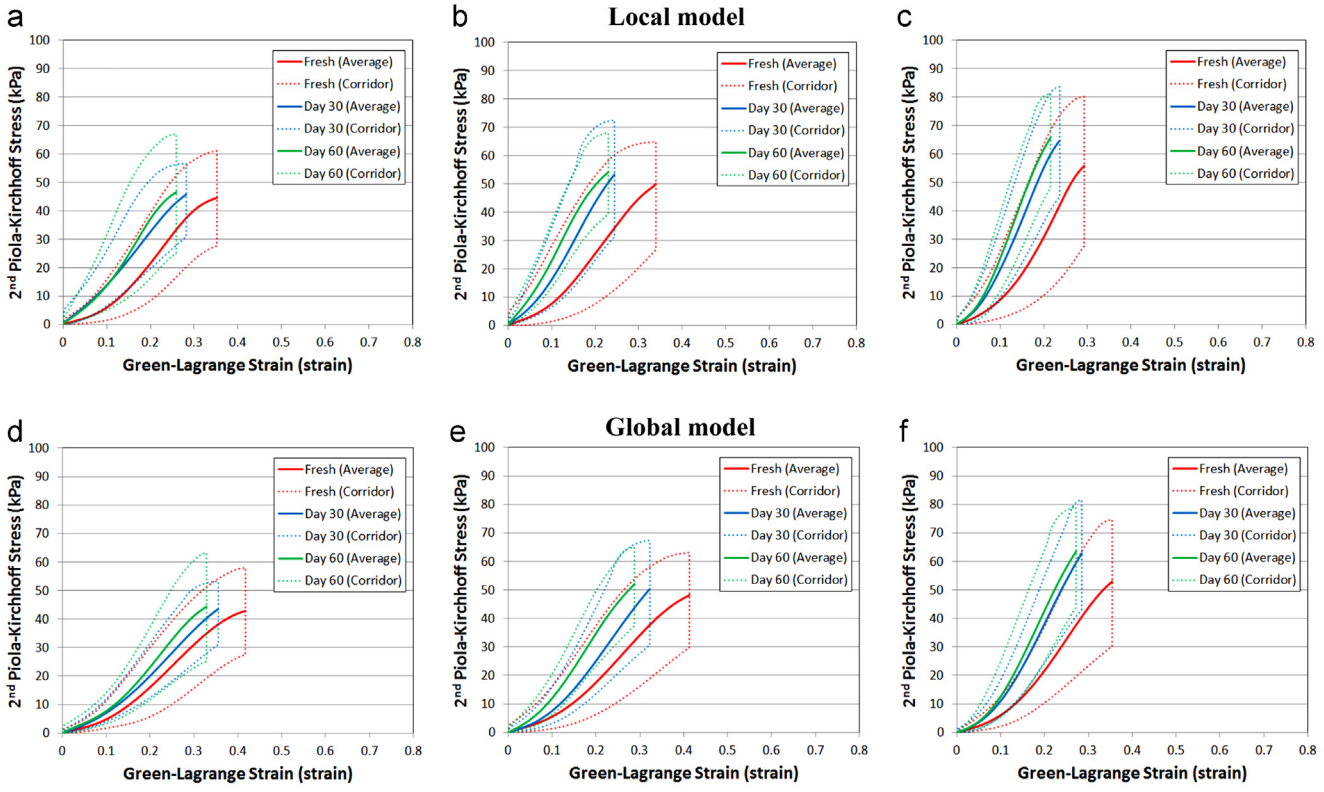

Fig. 5 – Characteristic averages and elliptical corridors of local model for (a) 0.01 s^{-1} (b) 0.1 s^{-1} and (c) 1 s^{-1} strain rates and of global model for (d) 0.01 s^{-1} (e) 0.1 s^{-1} and (f) 1 s^{-1} strain rates.

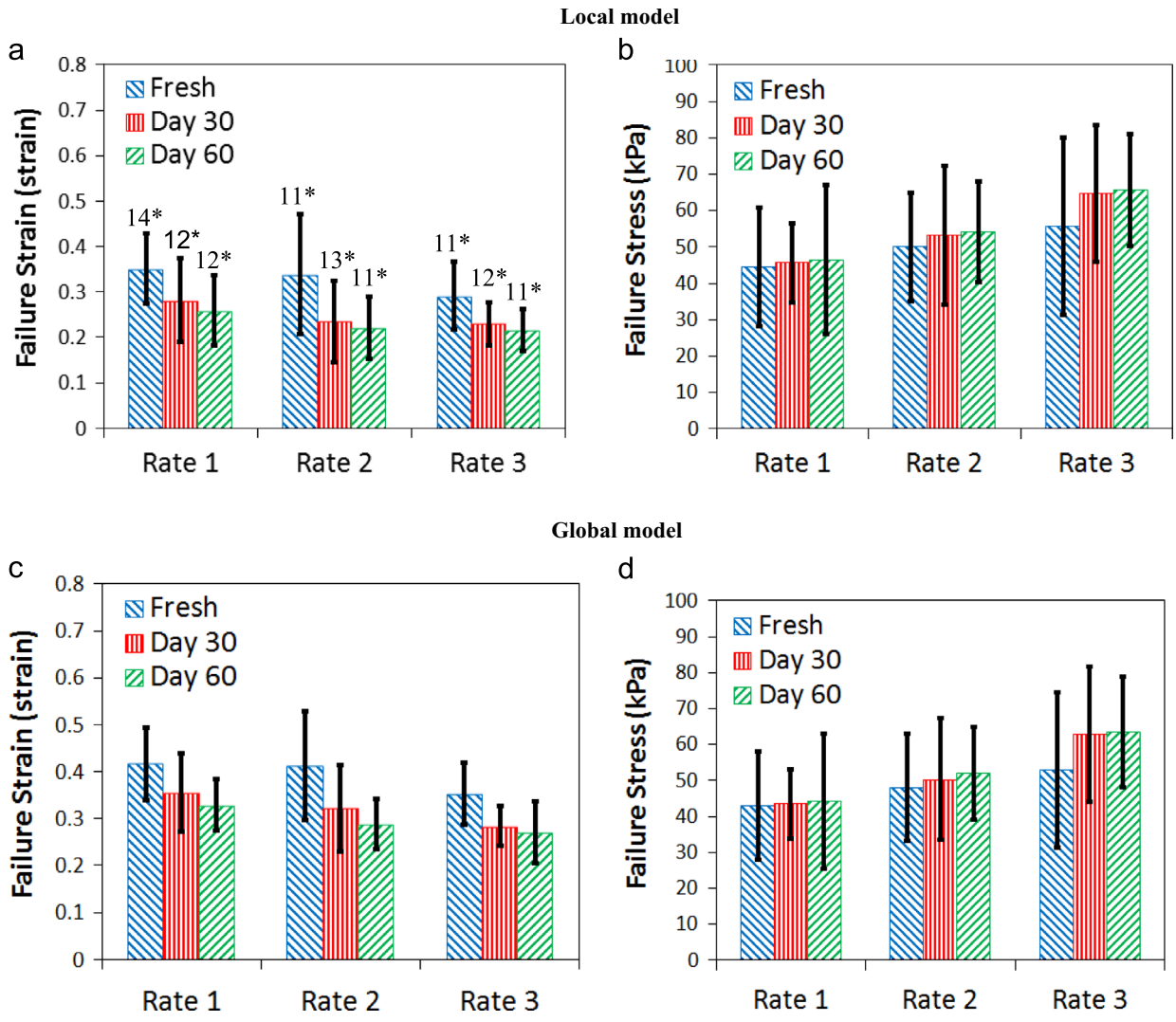

Fig. 6 – Failure stain and failure stress of the fresh and preserved tissues at three loading rates.

Table 2 – Statistical comparison (*p*-values from Mann–Whitney *U*-test) of failure strain between preservation times.

Comparison	Rate 1 Local/global	Rate 2 Local/global	Rate 3 Local/global
Fresh vs. Day 30	**0.037/0.033**	**0.049/0.049**	**0.029/0.007**
Fresh vs. Day 60	**0.015/0.002**	**0.036/0.013**	**0.018/0.015**
Day 30 vs. Day 60	0.707/0.544	0.772/0.385	0.601/0.559

Note: Bold: p-value < 0.05.

Table 3 – Statistical comparison (*p*-values from Mann–Whitney *U*-test) of failure stress between preservation times.

Comparison	Rate 1 Local/global	Rate 2 Local/global	Rate 3 Local/global
Fresh vs. Day 30	0.898/1.000	0.685/0.772	0.442/0.230
Fresh vs. Day 60	0.857/0.817	0.511/0.599	0.393/0.212
Day 30 vs. Day 60	0.403/0.403	1.000/0.954	0.926/0.878

in Fig. 6. The fresh specimens were found to have 17–44% higher failure strains than the Day 30 specimens and 27–50% higher failure strains than Day 60 specimens across all three loading rates for both LM and GM (Fig. 6a, c). The average failure stresses of preserved tissues where found to be larger than the average failure stresses of fresh tissues for both LM

Table 4 – Statistical comparison (p-values from Mann–Whitney U-test) of failure strain between rates.

Comparison	Fresh Local/global	Day 30 Local/global	Day 60 Local/global
Rate 1 vs. Rate 2	0.978/1.000	0.201/0.430	0.310/0.091
Rate 1 vs. Rate 3	0.059/0.059	0.157/**0.023**	0.132/**0.039**
Rate 2 vs. Rate 3	0.293/0.131	0.683/0.341	0.743/0.599

Note: Bold: p-value <0.05.

Table 5 – Statistical comparison (p-values from Mann–Whitney U-test) of failure stress between rates.

Comparison	Fresh Local/global	Day 30 Local/global	Day 60 Local/global
Rate 1 vs. Rate 2	0.311/0.338	0.265/0.221	0.148/0.148
Rate 1 vs. Rate 3	0.262/0.239	**0.007/0.009**	**0.011/0.011**
Rate 2 vs. Rate 3	0.743/0.646	0.165/0.183	0.168/0.237

Note: Bold: p-value <0.05.

Table 6 – The Ogden material model parameters of average stress–strain models for the three loading rates and preservation methods.

	Rate 1	Rate 2	Rate 3
	Fresh/Day 30/Day 60	Fresh/Day 30/Day 60	Fresh/Day 30/Day 60
Local			
α_1	8.51/7.52/8.49	9.00/9.72/6.45	11.86/10.44/10.69
μ_1 (kPa)	8.14/14.50/12.92	8.42/12.15/27.72	5.86/13.27/14.69
μ (kPa)	34.64/54.51/54.86	37.90/59.05/89.45	34.78/69.29/78.55
Global			
α_1	7.72/8.93/9.14	8.20/10.46/9.07	10.23/11.37/11.12
μ_1 (kPa)	7.79/6.97/7.55	7.65/6.25/10.95	5.95/7.77/9.00
μ (kPa)	30.10/31.12/34.50	31.36/32.71/49.62	30.43/44.17/50.08

and GM (Fig. 6b, d). The comparisons using paired two sample t-tests between LM and GM showed significant differences for all corresponding failure strain pairs and failure stress pairs ($p<0.05$), where the global failure strain was significantly higher and failure stress was significantly lower than the local values.

Statistical comparisons using Mann–Whitney tests showed significant differences in the failure strain between fresh and Day 30 specimens and between fresh and Day 60 specimens ($p<0.05$) for both LM and GM at all three loading rates (Table 2). However, the differences in failure strain between Day 30 specimens and Day 60 specimens were not significant ($p>0.05$). In addition, no significant differences were found for failure stress between fresh and preserved specimens or between storage times ($p>0.05$) (Table 3).

No significant differences in the failure strain or failure stress were found between loading rates for fresh tissues ($p>0.05$) (Tables 4–5). The only significant changes in preserved specimens were found between Rate 1 and Rate 3 in terms of the failure stress for both LM and GM ($p<0.05$), and failure strain for GM ($p<0.05$).

The optimal material model parameter α_1 ranged from 6.45 to 11.86, and μ_1 ranged from 5.86 to 27.72 kPa (Table 6). The ground-state shear modulus μ increased when comparing the preserved tissues to fresh tissues for both LM and GM at all three loading rates. The coefficients of determination (R^2) between the model force and experimental force were greater than 0.99 for all cases, indicating the good model fittings of the Ogden material model.

4. Discussion

Results demonstrated the failure strains of previously frozen bovine liver parenchyma were significantly different ($p<0.05$) from those of fresh liver parenchyma under tensile loading. Preservation by means of freezing resulted also in an increase in liver parenchyma stiffness. Significant differences between previously frozen bovine liver tissue and fresh bovine liver tissue have also been reported by previous studies (Brunon et al., 2010; Ocal et al., 2010; Santago et al., 2009). In addition, the failure properties and material model parameters were found to change with respect to the duration of frozen storage time. These observations can potentially be explained by the state of the cellular composition and architecture of the liver tissue during the freezing and thawing processes.

Extra-cellular and intra-cellular ice formation can be achieved by freezing the hepatic tissue to low temperatures (Mazur, 1977). Therefore, during freezing the expansion of the fluid and formation of irregularly shaped ice particles may damage the cell membranes and the connective tissue which binds the cells together, leading to a reduction in failure strain (Brunon et al., 2010; Ocal et al., 2010; Santago et al., 2009).

Although there have been some studies that have investigated the effect of freezing on liver tissue, the conclusions regarding the effect freezing on the material response of liver tissues varied between studies. A summary of various studies related to the comparison between fresh and frozen liver tissues is shown in Table 7. As can be observed, the majority of studies performed on porcine tissue have reported that the material properties of porcine liver are not affected by the freezing process. Conversely, the properties of bovine liver tissue have consistently been shown to be affected by the process of freezing in both tensile and compressive loading. This discrepancy could potentially be explained by the differences of the cellular architecture between porcine liver parenchyma and human/bovine liver parenchyma. Specifically, the lobules of porcine liver parenchyma are separated by relatively thick layers of collagenous septum, while the lobules of human and bovine liver are not (Eurell and Frappier, 2006; Matthews, 1971; Ross and Pawlina, 2006; Zhang, 1999). This accounts for the tougher nature of porcine liver compared to bovine liver (Eurell and Frappier, 2006). In addition, the majority of the porcine studies were performed with the capsule attached to the parenchyma. Tamura et al. (2002) is the only study which quantified the effect of freezing on the compressive properties of isolated porcine liver parenchyma. Tamura et al., (2002) concluded that freezing does not affect the compressive repose of porcine liver parenchyma based on the response of matched specimens after 5 cycles of sub-failure preconditioning. However, it is possible that damaged incurred by the tissue during the preconditioning may have masked any possible changes in the compressive response resulting from the freezing process. It is also possible that the compressive material properties of liver parenchyma are not as sensitive to the effects of freezing as the tensile material properties since the mechanics of compressing cells together are fundamentally different than the mechanics of pulling cells apart. Overall, based on the summary and comparison of the various studies which have investigated the effect of freezing on liver tissue it is reasonable to conclude that while porcine liver material properties are generally unaffected by the process of freezing, the tensile and compressive material properties of bovine liver parenchyma are significantly affected by the process of freezing.

With respect to the loading rate, the failure strain significantly decreased while the failure stress significantly increased with increased loading rate for previously frozen tissues ($p<0.05$). However, there were no statistically significant differences found for fresh tissues with respect to loading rate ($p>0.05$). This is consistent with the finding of Kemper et al. (2010), who reported that while the tensile failure stress and failure strain of fresh human liver parenchyma increased with respect to loading rate there were not significant differences between loading rates of approximately 0.01 s^{-1}, 0.1 s^{-1}, and 1 s^{-1}. However, Kemper et al. (2010) did report that the tensile failure stress significantly increased and the failure strain significantly decreased between loading rates of 0.01 s^{-1} and 10.0 s^{-1}. In addition, the comparisons of failure strain and failure stress between the fresh bovine liver parenchyma in the current study and fresh human liver parenchyma in the study conducted by Kemper et al. (2010) using Mann–Whitney tests showed no significant differences ($p>0.05$) for all three loading rates, which is consistent with the findings of Kemper et al., (2010) (Fig. 7). Therefore, bovine liver tissues may serve as a reasonable surrogate for human liver tissues when investigating the tensile mechanical properties at various loading rates (0.01–1.0 s^{-1}).

Although there were some observed differences in the failure stress and failure strain between the local and global models (LM and GM), the tissue preservation and rate-dependency comparisons showed the same effect on the changes in the failure properties for both models. As in our previous study (Untaroiu and Lu, 2013), significantly larger failure strains and lower failure stresses were observed in the global model compared to the local model for all three loading rates and preservation scenarios ($p<0.05$). These differences could be caused by the inhomogeneity of the tissue material properties or irregularity of the cross-sectional areas within the gage

Table 7 – Comparison of the freezing effect on liver tissues between studies.

Study	Source	Type	Loading	Specimen	Comparison	Effect of freezing
Brunon et al. (2010)	Human	Tension	0.001 s^{-1}-0.01 s^{-1}	Capsule+parenchyma	Fresh, 24 h	No
Brunon et al. (2010)	Porcine	Tension	0.001 s^{-1}-0.01 s^{-1}	Capsule+parenchyma	Fresh, 24 h	Yes
Lu and Untaroiu (2013)	Porcine	Indentation	0.5 mm/s	Capsule+parenchyma	Fresh, Day 20	No
Nguyen et al. (2012)	Porcine	Tension	0.08 s^{-1}	Capsule+parenchyma	Fresh, 48 h	No
Tamura et al. (2002)	Porcine	Compression	0.5 mm/s	Parenchyma	Fresh, 24 h	No
Ocal et al. (2010)	Bovine	Compression	48 mm/s	Parenchyma	Fresh, 1–48 h	Yes
Santago et al. (2009)	Bovine	Tension	0.07 s^{-1}	Parenchyma	Fresh, Day 26	Yes
Current study	Bovine	Tension	0.01 s^{-1}, 0.1 s^{-1}, 1.0 s^{-1}	Parenchyma	Fresh, Day 30, Day 60	Yes

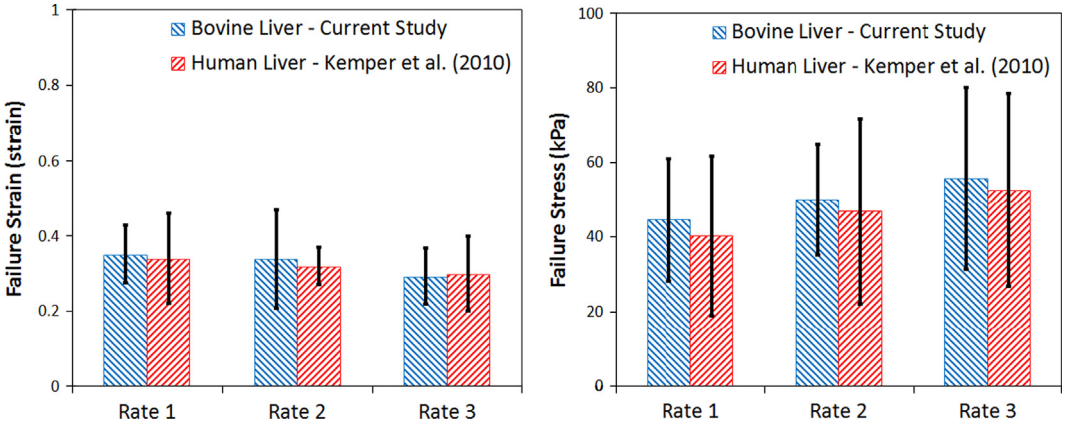

Fig. 7 – Comparison of tensile failure strain between bovine and human livers.

length. However, it is more likely that the majority of differences between the local and global models are due to the fact that the global model does not account for the variation in cross-sectional area outside of the gage length (i.e. the fillets between the gage length and grip area), or the complex state of stress in the fillet area due to the compressive stress imposed on the tissue by the grips.

In the current study, the isolated specimens of liver parenchyma of the liver were tested without the liver capsule attached, which is similar to other studies performed on bovine liver tissue (Kemper et al., 2010; Pervin et al., 2011; Santago et al., 2009). However, some previous studies using bovine liver have shown that the material properties of the capsule are different than that of the parenchyma (Hollenstein et al., 2006; Untaroiu and Lu, 2013). The hepatic capsule surrounding the liver is composed of a tough fibrous layer enriched with collagen and elastin. It was reported that a decomposition of elastin during the periods of thawing at room temperature could change the stiffness of the tissue, making the organ more rigid (Eichberger et al., 2000; Manoogian et al., 2009; Snedeker et al., 2005). Therefore, future studies should be performed to evaluate the effect of different storage conditions on the material properties of the capsule surrounding the liver. The results from such a study would allow the mechanical behavior of capsule and parenchyma to be modeled individually, which may lead to more accurate computational models (e.g. in FE models) of the liver as a whole. In addition, the rate dependency of liver parenchyma could be assigned to FE liver models using a new LS-Dyna material model (MAT_181) (Hallquist, 2007), which employs a tabulated formulation of hyper-elasticity with rate effects (Pervin et al., 2011; Untaroiu and Lu, 2013). In the future, this data may be used in FE simulations to investigate the differences in global behavior of fresh and preserved PMHS.

As with any study of material properties of soft tissues, this study has some limitations. First, both GM and LM models assumed constant cross-sectional area (A_0) which means a constant strain distribution along the tissue. A more delicate approach called specimen-specific FE modeling, utilizing the original shapes of the dog-bone specimens, could be applied to obtain more accurate model parameters (Hu et al., 2009, 2011; Klinich et al., 2012; Untaroiu, 2013; Untaroiu and Lu, 2013). In addition, while the current study has evaluated the effect of different frozen storage times relative to fresh tissue, there is a lack of data regarding the effect of different storage conditions (e.g. storage temperatures) on the mechanical properties of bovine and human abdominal tissues in tensile loading (Lu and Untaroiu, 2013), and these are suggested to be investigated in the future.

Several non-invasive methods (e.g. elastography) have been applied during *in vivo* tests, primarily for the detection of liver fibrosis in patients (Huwart et al., 2006; Rouvière et al., 2006). However, the values of shear modulus reported by these studies (2–6 kPa) are generally lower than the corresponding data reported from mechanical *in vitro* testing. These differences could be associated with the approximations of the liver tissue used to solve the shear wave equation (e.g. purely elastic, isotropic, infinite, and homogenous) (Bercoff et al., 2004), and with the different environmental conditions (e.g. *in vivo*, *in situ*, and *ex vivo*). In addition, these *in vivo* methods only generate finite strains in the liver tissue, which are likely well within the toe region of the stress–strain curve. Therefore, more effort should be placed on improving the understanding of *in vivo* liver properties in order to improve the biofidelity of liver material models.

5. Conclusions

The current study quantified the material and failure response of fresh and preserved liver parenchyma specimens in tensile loading at various strain rates. Significant changes in the failure strain were observed between previously frozen liver parenchyma samples and fresh samples at both global and local levels ($p<0.05$). In addition, nonlinear and viscoelastic characteristics of the liver parenchyma were observed for both fresh and preserved samples. Specifically, the failure strain of preserved bovine liver specimens decreased while the failure stress increased with increased loading rate. Although fresh liver specimens demonstrated a similar trend with respect to loading rate, the changes in the failure stress

and strain of fresh tissues were not significant for various loading rates evaluated in the current study ($p>0.05$). It is believed that with continued development of abdominal organ material models, such as the one presented in the current study, will lead to improved whole body FE models that will aid in the prediction and prevention of abdominal injuries resulting from blunt trauma.

REFERENCES

Arajarvi, E., Santavirta, S., Tolonen, J., 1987. Abdominal injuries sustained in severe traffic accidents by seatbelt wearers. Journal of Trauma 27, 393–397.

Bercoff, J., Tanter, M., Fink, M., 2004. Supersonic shear imaging: a new technique for soft tissue elasticity mapping. IEEE Transactions on Ultrasonics, Ferroelectrics, and Frequency Control 51, 396–409.

Brammer, R.D., Bramhall, S.R., Mirza, D.F., Mayer, A.D., McMaster, P., Buckels, J.A., 2002. A 10-year experience of complex liver trauma. British Journal of Surgery 89, 1532–1537.

Brunon, A., Bruyere-Garnier, K., Coret, M., 2010. Mechanical characterization of liver capsule through uniaxial quasi-static tensile tests until failure. Journal of Biomechanics 43, 2221–2227.

Bummo, A., Jung, K., 2007. An efficient soft tissue characterization method for haptic rendering of soft tissue deformation in medical simulation. Frontiers in the Convergence of Bioscience and Information Technologies 2007 (2007), 549–553.

Cheynel, N., Gentil, J., Freitz, M., Rat, P., Ortega Deballon, P., Bonithon Kopp, C., 2011. Abdominal and pelvic injuries caused by road traffic accidents: characteristics and outcomes in a french cohort of 2009 casualties. World Journal of Surgical 35, 1621–1625.

Chui, C., Kobayashi, E., Chen, X., Hisada, T., Sakuma, I., 2007. Transversely isotropic properties of porcine liver tissue: experiments and constitutive modelling. Medical and Biological Engineering and Computing 45, 99–106.

Coleman, T., 2011. Matlab Optimization Toolbox User's Guide. R2011b ednR2011b ed. The MathWorks, Inc., Natick, MA.

Crandall, J.R., 1994. Preservation of Human Surrogates for Impact Studies. University of Virginia, Charlottesville, VA, US.

Crandall, J.R., Bose, D., Forman, J., Arregui-Dalmases, C., Untaroiu, C.D., Shaw, C.G., Kerrigan, J.R., 2011. A review of human surrogates for injury biomechanics research. Clinical Anatomy 24, 362–371.

Eichberger, A., Darok, M., Steffan, H., Leinzinger, P.E., Bostrom, O., Svensson, M.Y., 2000. Pressure measurements in the spinal canal of post-mortem human subjects during rear-end impact and correlation of results to the neck injury criterion. Accident Analysis and Prevention 32, 251–260.

Elhagediab A., Rouhana S., 1998. Patterns of abdominal injury in frontal automotive crashes. In: Proceedings of the 16th International Technical Conference on the Enhanced Safety of Vehicles, Windsor, Ontario, Canada.

Eurell, J.A., Frappier, B.L., 2006. Dellmann's Textbook of Veterinary Histology, 6th ed. Wiley-Blackwell, Hoboken, NJ, US.

Frankel, V.H., 1960. The Femoral Neck: an Experimental Study of Function, Fracture Mechanism, and Internal Fixation. Almqvist and Wiksells, Stockholm, Sweden.

Greingor, J.L., Lazarus, S., 2006. Chest and abdominal injuries caused by seat belt wearing. Southern Medical Journal 99, 534–535.

Griffon, D.F., Wallace, L.F., Bechtold, J.E., 1995. Biomechanical properties of canine corticocancellous bone frozen in normal saline solution. American Journal of Veterinary Research 56, 822–825.

Hallquist, J.O., 2007. Ls-Dyna Keyword User's Manual, LSTC, Livermore, CA, USA.

Hamer, A.J., Strachan, J.R., Black, M.M., Ibbotson, C.J., Stockley, I., Elson, R.A., 1996. Biomechanical properties of cortical allograft bone using a new method of bone strength measurement: a comparison of fresh, fresh-frozen and irradiated bone. Journal of Bone and Joint Surgery, British Volume78-B, 363–368.

Hollenstein, M., Nava, A., Valtorta, D., Snedeker, J.G., Mazza, E., 2006. Mechanical characterization of the liver capsule and parenchyma. In: Harders, Matthias, Gábor, Székely (Eds.), Biomedical Simulation. Springer, Berlin Heidelberg, pp. 150–158.

Holzapfel, G.A., 2000. Nonlinear Solid Mechanics: A Continuum Approach for Engineering, 1st ed. Wiley, Chichester, UK.

Hu, J., Klinich, K.D., Miller, C.S., Nazmi, G., Pearlman, M.D., Schneider, L.W., Rupp, J.D., 2009. Quantifying dynamic mechanical properties of human placenta tissue using optimization techniques with specimen-specific finite-element models. Journal of Biomechanics 42, 2528–2534.

Hu, J., Klinich, K.D., Miller, C.S., Rupp, J.D., Nazmi, G., Pearlman, M.D., Schneider, L.W., 2011. A stochastic visco-hyperelastic model of human placenta tissue for finite element crash simulations. Annals of Biomedical Engineering 39, 1074–1083.

Huwart, L., Peeters, F., Sinkus, R., Annet, L., Salameh, N., ter Beek, L.C., Horsmans, Y., Van Beers, B.E., 2006. Liver fibrosis: non-invasive assessment with MR elastography. NMR in Biomedicine 19, 173–179.

Kemper, A.R., Santago, A.C., Stitzel, J.D., Sparks, J.L., Duma, S., 2010. Biomechanical response of human liver in tensile loading. Annals of Advances in Automotive Medicine 54, 15–26.

Kemper, A.R., Santago, A.C., Stitzel, J.D., Sparks, J.L., Duma, S.M., 2012. Biomechanical response of human spleen in tensile loading. Journal of Biomechanics 45, 348–355.

Klinich, K.D., Miller, C.S., Hu, J., Samorezov, J.E., Pearlman, M.D., Schneider, L.W., Rupp, J.D., 2012. Characterization of ovine utero-placental interface tensile failure. Placenta 33, 776–781.

Lessley D., Crandall J.R., Shaw G., Kent R.W., Funk J., 2004. A Normalization Technique for Developing Corridors from Individual Subject Responses, SAE Technical Paper, 2004-01-0288.

Linde, F., Sorensen, H.C., 1993. The effect of different storage methods on the mechanical properties of trabecular bone. Journal of Biomechanics 26, 1249–1252.

Lu, Y.-C., Untaroiu, C.D., 2013. Effect of storage methods on indentation-based material properties of abdominal organs. Proceedings of the Institution of Mechanical Engineers, Part H: Journal of Engineering in Medicine 227, 293–301.

Manoogian, S.J., Bisplinghoff, J.A., McNally, C., Kemper, A.R., Santago, A.C., Duma, S.M., 2009. Effect of strain rate on the tensile material properties of human placenta. Journal of Biomechanical Engineering 131, 091008.

Matthews, J., 1971. In: Atlas of Human Histology and Ultrastructure. Lea and Febiger, Philadelphia.

Mazur, P., 1977. The role of intracellular freezing in the death of cells cooled at supraoptimal rates. Cryobiology 14, 251–272.

McIntosh, A.S., Kallieris, D., Frechede, B., 2007. Neck injury tolerance under inertial loads in side impacts. Accident Analysis and Prevention 39, 326–333.

Nava, A., Mazza, E., Furrer, M., Villiger, P., Reinhart, W.H., 2008. In vivo mechanical characterization of human liver. Medical Image Analysis 12, 203–216.

Nguyen, N.H., Du'o'ng, M.T., Tran, T.N., Pham, P.T., Grottke, O., Tolba, R., Staat, M., 2012. Influence of a freeze-thaw cycle on the stress–stretch curves of tissues of porcine abdominal organs. Journal of Biomechanics 45, 2382–2386.

Ocal, S., Ozcan, M.U., Basdogan, I., Basdogan, C., 2010. Effect of preservation period on the viscoelastic material properties of soft tissues with implications for liver transplantation. Journal of Biomechanical Engineering 132, 101007.

Ogden, R.W., 1997. In: Non-Linear Elastic Deformations. Dover Publications, Mineola, NY.

Pervin, F., Chen, W.W., Weerasooriya, T., 2011. Dynamic compressive response of bovine liver tissues. Journal of the Mechanical Behavior of Biomedical Materials 4, 76–84.

Ross, M.H., Pawlina, W., 2006. Histology: A Text and Atlas: With Correlated Cell and Molecular Biology, 5th ed. Lippincott Williams and Wilkins, Baltimore.

Rouvière, O., Yin, M., Dresner, M.A., Rossman, P.J., Burgart, L.J., Fidler, J.L., Ehman, R.L., 2006. MR elastography of the liver: preliminary results. Radiology 240, 440–448.

Salzar, R.S., Bass, C.R., Lessley, D., Crandall, J.R., Kent, R.W., Bolton, J.R., 2009. Viscoelastic response of the thorax under dynamic belt loading. Traffic Injury Prevention 10, 290–296.

Santago, A.C., Kemper, A.R., McNally, C., Sparks, J.L., Duma, S., 2009. Freezing affects the mechanical properties of bovine liver. Biomedical Sciences Instrumentation 45, 24–29.

Sedlin, E.D., 1965. A rheological model for cortical bone. Acta Orthopaedica Scandinavica 83.

Smeathers, J.E., Joanes, D.N., 1988. Dynamic compressive properties of human lumbar intervertebral joints: a comparison between fresh and thawed specimens. Journal of Biomechanics 21, 425–433.

Snedeker, J.G., Niederer, P., Schmidlin, F.R., Farshad, M., Demetropoulos, C.K., Lee, J.B., Yang, K.H., 2005. Strain-rate dependent material properties of the porcine and human kidney capsule. Journal of Biomechanics 38, 1011–1021.

Tamura, A., Omori, K., Miki, K., Lee, J.B., Yang, K.H., King, A.I., 2002. Mechanical characterization of porcine abdominal organs. Stapp Car Crash Journal 46, 55–69.

Untaroiu, C.D., 2013. The influence of the specimen shape and loading conditions on the parameter identification of a viscoelastic brain model. Computational and Mathematical Methods in Medicine 2013, 460413.

Untaroiu, C.D., Lu, Y.-C., 2013. Material Characterization of liver parenchyma using specimen-specific finite element models. Journal of the Mechanical Behavior of Biomedical Materials 26, 11–22.

Untaroiu, C.D., Bose, D., Lu, Y.-C., Riley, P., Lessley, D., Sochor, M., 2012. Effect of seat belt pretensioners on human abdomen and thorax: biomechanical response and risk of injuries. Journal of Trauma and Acute Care Surgery 72, 1304–1315.

Weaver, J.K., 1966. The microscopic hardness of bone. Journal of Bone and Joint Surgery 48, 273–288.

Woo, S.L., Orlando, C.A., Camp, J.F., Akeson, W.H., 1986. Effects of postmortem storage by freezing on ligament tensile behavior. Journal of Biomechanics 19, 399–404.

Zhang, S.-X., 1999. In: An Atlas of Histology. Springer, New York.